Journal of
Materials Chemistry A

RSC Publishing

PAPER

View Article Online
View Journal | View Issue

Cite this: *J. Mater. Chem. A*, 2013, **1**, 13139

Graphene modified carbon nanosheets for electrochemical detection of Pb(II) in water

Jin-Tao Zhang, Zhen-Yu Jin, Wen-Cui Li, Wei Dong and An-Hui Lu*

Received 5th July 2013
Accepted 2nd September 2013

DOI: 10.1039/c3ta12612a

www.rsc.org/MaterialsA

A novel graphene modified carbon nanosheet (GMCN) was constructed by using graphene oxide as the shape-directing agent, and resorcinol and formaldehyde as carbon precursors through a surface assembly process. The GMCN can be used as an efficient electrochemical sensing material for Pb(II) detection in an aqueous solution using square wave anodic stripping voltammetry. Due to the efficient integration of porous features of the resin-based carbon and the excellent electrical conductivity of graphene, such materials possess a superior adsorption capacity and fast electron-transfer kinetics. The sensitivity is as high as 92.86 μA μmol^{-1} and a limit of detection as low as 1.12 nM has been reached. The thickness of the carbon nanosheets can be tuned by varying the reactant mass ratio, which ensures a tuneable electrical conductivity and surface area. A good balance between electrical conductivity and surface area allows a high adsorption capacity towards Pb(II), high signal-to-background ratio and rapid electron and ion diffusion paths for electrochemical reactions as well, which significantly improves the electrochemical sensing performance in the detection of Pb(II). Potentially, such nanosheet materials can be used in the field of heavy metal ion detection.

1 Introduction

Heavy metal pollution is known to be one of the most serious pollution problems in nature due to the stability of metals at contaminated sites and high toxicity to the biosphere.[1,2] It is very important to develop a rapid, sensitive, and simple analytical method for the detection and monitoring of these toxic metal ions.[3,4] Atomic absorption spectrometry, UV-Vis spectroscopy and inductively coupled plasma mass spectrometry are the main existing techniques for the analysis of heavy metal ions. Because of the dependence on bulky and complicated instruments, the existing methods involve significant drawbacks, such as time consumption, high operating costs and unsuitability for on-field analysis.[5] In contrast, as an alternative to these existing techniques, square wave anodic stripping voltammetry (SWASV) provides a powerful tool for the detection of heavy metal ions, which possesses the advantages of high-sensitivity, low operating cost, fast response and portability.[6–8] As is known, its sensing performance mainly depends on the accumulation of target ions on the surface of the electrode and the electron transfer between the material and the electrode, and is therefore closely associated with the adsorption capacity and electro-activity of the sensing material modified on the electrode.[9] Therefore, a study on the electrochemical sensors based on a novel material with excellent sensing performance towards the heavy metal ions should be of great interest and significance.

Widespread attention has been paid to the nanomaterials with high adsorption capacity, which makes them suitable for electrochemical detection of heavy metal ions.[10–14] To enhance the efficiency of accumulating target ions on the surface of electrodes, porous carbons have been selected as active materials to modify the electrodes.[15–17] Owing to their high surface area, developed porous structures and abundant surface functional groups, porous carbons exhibit high removal capacities and fast adsorption rates for heavy metal ions. Despite so many advantages of porous carbons, the porosity together with their higher electrical resistance compared to that of graphene hinder the electron transfer between the sensing materials and the electrode, which may restrict their sensing application. In recent reports, unmodified carbon nanotubes (CNTs) have also attracted scientists as novel electrode materials due to their excellent electrochemical features: a large potential window and a fast electron transfer rate.[18,19] However, poor binding capacity of unmodified CNTs towards Pb(II) inevitably decreases the efficiency of accumulating target analytes on an electrode surface, which may have a negative influence on further improvement of the detection sensitivity.[20–23] Thus, further studies are still necessary to provide more insights into the synthesis of an efficient and suitable nanomaterial.

Graphene, a single-atom-thick two-dimensional carbon material, has been considered as an ideal platform for the highly sensitive detection of the heavy metals in terms of

State Key Laboratory of Fine Chemicals, School of Chemical Engineering, Faculty of Chemical, Environmental and Biological Science and Technology, Dalian University of Technology, Dalian 116024, P.R. China. E-mail: anhuilu@dlut.edu.cn; Fax: +86-411-84986112; Tel: +86-411-84986112

extraordinary electronic transport properties,[24] large surface-to-volume ratios[25–27] and high electrocatalytic activities.[28] In addition, graphene-based nanocomposites show significant improvement in properties that cannot normally be achieved using conventional composites or pure graphene oxide (GO).[29–31] Recently, many graphene-based sensors have been constructed for electrochemical sensing of heavy metal ions, such as graphene decorated with metal oxides and conducting polymers.[32–35]

Herein, we have combined the advantages of the high adsorption capacity of porous carbons and the layered structure and excellent electrical conductivity of graphene to fabricate a sensing platform for detection of Pb(II) in a solution by SWASV. In this work, we have synthesized this new material of graphene modified carbon nanosheets (GMCN). During the synthesis process, a small amount of layered GO (1.1 wt% to 6.2 wt%) was used mainly as the shape-directing agent to induce the assembly of porous carbon nanosheet structures, and meanwhile as conductive additives (after reduction in the pyrolysis) to improve the electric conductivity of porous carbon. The graphene modified carbon nanosheets demonstrated a good balance between the electrical conductivity and surface area, which is crucial for an excellent sensitivity and detection limit. Moreover, compared to the polymer/graphene composite[36] and metal oxide/graphene[45] used in detection of heavy metal ions in waste water, graphene modified porous carbon with good chemical stability[37] can be applied under harsh conditions, for example, strong acid or base.

2 Experimental section

2.1 Chemicals

Resorcinol (denoted as R, 99.5%) was purchased from Tianjin Kermel Chemical Reagent Co., Ltd. Asparagine (denoted as Asn, 99.5%) was purchased from Fluka. Formalin (37 wt%), anhydrous sodium acetate (NaAc), acetic acid (HAc), and lead nitrate ($Pb(NO_3)_2$) were supplied by Sinopharm Chemical Reagent Co., Ltd. GO colloids used in this work were prepared by following a modified Hummer's method.

2.2 Preparation of GMCNs

Graphene modified carbon nanosheets (GMCNs) were prepared according to the process reported previously by our group. In brief, 0.23 g Asn was first dissolved in 26 mL GO colloids (1.8 mg mL^{-1}) at 25 °C. After complete dissolution, 0.75 g resorcinol was added to the above solution and stirred for *ca.* 5 min. Subsequently, 1.106 g formalin (37 wt%) was quickly injected into the solution. The homogeneous solution was then sealed and transferred into an oven at 90 °C for 18 h. The obtained polymer gel was dried at room temperature, followed by pyrolysis at 800 °C for 2 h under a nitrogen atmosphere to obtain GMCN-2. By varying the mass ratio between the carbon precursor and GO of 15.1 : 1, 25.3 : 1, 45.7 : 1 and 86.5 : 1, four samples (denoted as GMCN-1, GMCN-2, GMCN-3 and GMCN-4) with different thickness of carbon sheets were prepared, in which the mass of GO is constant.

2.3 Electrode fabrication

The construction of the GMCN film on the surface of glassy carbon electrodes was performed as follows: 5 mg sample was suspended in 1 mL ethanol to form a suspension. The suspension was then briefly sonicated for 30 s in order to disperse the microspheres. A 5 μL aliquot of this suspension was then pipetted onto the surface of a freshly polished glassy carbon electrode. And then a drop of the Nafion solution (5 μL, 0.5 wt%) was placed on the electrode surface and the solvents were left to evaporate at room temperature.[38]

2.4 Characterization

Scanning electron microscopy (SEM) investigations for the GMCN were carried out with a NOVA NanoSEM 450 instrument. X-ray diffraction (XRD) patterns of samples were recorded with a Rigaku D/Max 2400 diffractometer in the Bragg Brentano (reflection) geometry using Cu Kα radiation ($\lambda = 0.15406$ nm). Nitrogen sorption isotherms were measured with a Micromeritics TriStar 3000 physisorption analyzer. The Brunauer–Emmett–Teller (BET) method was utilized to calculate the specific surface areas (S_{BET}). Total pore volumes (V_{total}) were calculated from the amount adsorbed at a relative pressure P/P_0 of 0.97. Micropore volumes (V_{micro}) were calculated using the *t*-plot method. The pore size distributions were determined based on the density function theory (DFT) model.

2.5 Analytical experiments

All electrochemical measurements were performed using a CHI 660D (Shanghai CH Instruments, China) Electrochemical Workstation. Square wave anodic stripping voltammetry (SWASV) was used for the observation of electrochemical behavior under optimized conditions. Pb(II) was deposited at a potential of −1.2 V for 400 s by the reduction of Cd(II) and Pb(II) in 1 M NaAc–HAc (pH = 5.5). The anodic stripping (reoxidation of metal to metal ions) of electrodeposited metal was performed in the potential range of −0.9 to −0.3 V at the following parameters: frequency, 15 Hz; amplitude, 25 mV; increment potential, 4 mV. The sample metal deposited on the electrode surface was removed by electrolysis at 0.3 V for 120 s in a fresh supporting electrolyte prior to the next cycle.

3 Results and discussion

3.1 Structures of graphene modified carbon nanosheets

Field-emission scanning electron micrographs (FE-SEM) throw light on the direct and visual structural characteristics of the as-synthesized GMCN. As shown in Fig. 1, our samples exhibit uniformly layered structures, and according to our previous work,[40] the GO macromolecules serve as the shape and structure directing roles during the surface assembly process, leading to uniformly layered structures. Very intriguingly, the carbon sheets are remarkably smooth, and their average thicknesses are measured to be 10 ± 2, 20 ± 2, 34 ± 4 and 72 ± 6 nm, respectively. As is seen, the interspace between the carbon sheets leads to the formation of developed macropores and layered structures which lead to exposure of the large surface

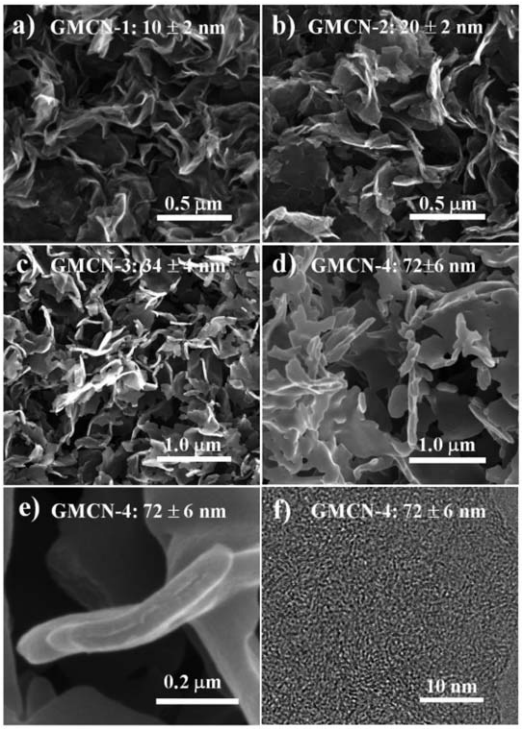

Fig. 1 FE-SEM and TEM images of the as-prepared GMCN samples with different average thickness of carbon sheets.

area, and may enhance Pb(II) diffusion kinetics. It is noteworthy that we could alter the layer thickness continuously over a wide range of 10–80 nm by changing the reactants' mass ratio, achieving shape-controllable synthesis of our samples. As shown in Fig. 1e, GMCN-4 exhibits a carbon–graphene hybrid structure with a centred graphene layer and two microporous carbon layers on both sides. Meanwhile, the high resolution TEM image (Fig. 1f) shows its dominating amorphous feature (rich micropores), which confirms its porous structure.

To gain further insight into the microstructure information of GMCNs, powder X-ray diffraction (XRD) characterization was employed to monitor the phase structure of the different samples (Fig. 2a). In an XRD pattern of the obtained GO sample, a sharp peak centered at $2\theta = 10.6°$ was observed, corresponding to the (001) interplanar spacing of 0.83 nm. The absence of the characteristic peak of pristine graphite at $2\theta = 26.4°$ suggested that the graphite was successfully converted into graphene oxide after oxidation using Hummer's method.[39] After hydrothermal reduction, GO was converted into reduced graphene nanosheets as evidenced by XRD patterns. In the cases of GMCNs before and after pyrolysis, the appearance of the broad peaks in the range of $2\theta = 10$–$30°$ indicates the amorphous structure of the sample, demonstrating layered graphene percolation in the polymer and carbon matrix.[40] Because of the extraordinary electronic transport properties of graphene, one can thus envisage that our GMCN would show better electrical conductivity than pure microporous carbon, and the improved electrochemical properties might provide an opportunity in sensing applications.

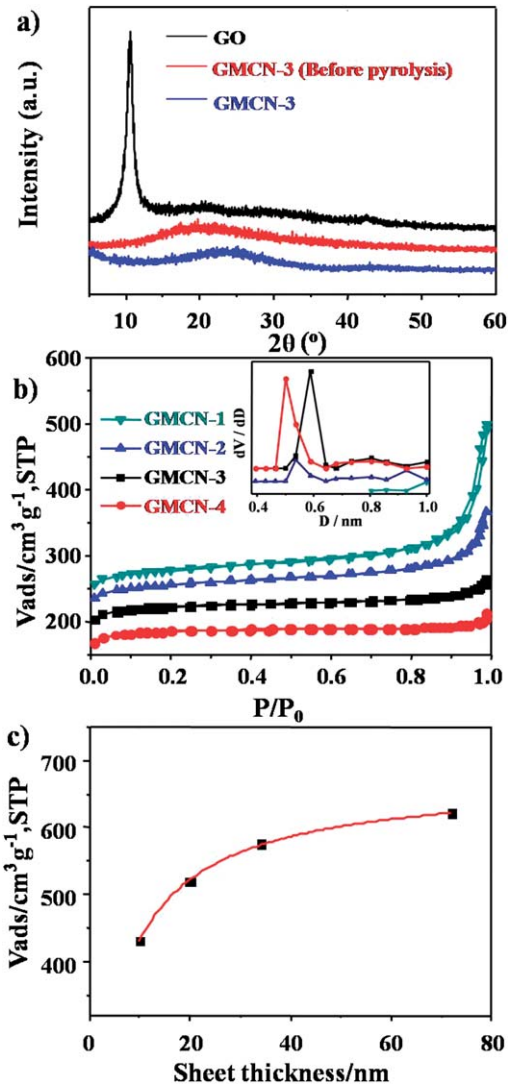

Fig. 2 The structure analysis. (a) The XRD patterns of GO and the as-made GMCN before and after carbonization. (b) The N_2 adsorption isotherms and pore size distribution of the as-made GMCN samples. The isotherms of GMCN-1, GMCN-2 and GMCN-3 are vertically offset by 150, 100, and 50 $cm^3\ g^{-1}$, at STP, respectively. (c) The relationship between the thickness of sheets and the surface area of GMCNs.

For the sake of further analysis of the pore structure, we conducted N_2 physisorption experiments, and the rich porosity on the nanometer scale of our GMCN was confirmed by the corresponding N_2 adsorption–desorption isotherms (Fig. 2b). The adsorption isotherms are the combination of types I and II, which show micropore filling and inter-particle capillary condensation (according to the IUPAC classification). In the lower relative pressure range ($P/P_0 < 0.1$), the significant N_2 uptake is associated with the rich microporosity. The pore size distribution tends to concentrate on 0.5–0.6 nm (Fig. 2b, inset) with increase of the mass ratio between the carbon precursor and GO. Such an amorphous carbon coating on graphene sheets allows the formation of micropores during pyrolysis, while the macropores can be mainly related to the interspace between the carbon nanosheets, as observed by SEM. Together

with the SEM observation, one can conclude that our GMCNs possess a micro/macropore system. Similar to some similar 3D interconnected graphene hydrogels,[41] the remarkable advantage of a hierarchically interconnected pore system is that the mass transportation is facile, favorable for fast adsorption rates for heavy metal ions.

The structure parameters are listed in Table 1. It was observed that, among the four samples, GMCN-4 with the thickest sheets showed the highest surface area of 621 $m^2\ g^{-1}$, followed by GMCN-3 (576 $m^2\ g^{-1}$), GMCN-2 (520 $m^2\ g^{-1}$) and GMCN-1 (431 $m^2\ g^{-1}$) with the thinnest sheets. In order to further study the surface area of the material in relation to the thickness of the materials, the fitted curves could be achieved as shown in Fig. 2c. From the fitted curves, it can be seen that the surface area was improved with increasing sheet thickness, rapidly in the initial stages, and the tendency slowed down when the sheets became thick. The surface area of GMCNs is mainly derived from the microporous carbon. The obtained surface area can be comparable to the reported PEI-cross-linked GO aerogels[42] and covalently cross-linked resorcinol–formaldehyde porous carbon (made in-house), which further confirms the role of porous carbon. Considering the large surface area of such microporous carbon, it has been recognized that the strong adsorption ability might perform well for sensing applications.

Graphene has good conductivity, while the microporous carbon layers have good adsorbability towards the target heavy metal ions but poor conductivity. The aforementioned characterization results verified that the current synthesis was effective and facile to fabricate samples with high surface area and good conductivity. Furthermore, the thickness of the microporous carbon sheets has a strong impact on the surface areas of our samples. Simultaneously, the electrical conductivity of these samples is also determined by the thickness of the carbon sheets, which is proven in the Electrochemical characterization of GMCN section.

3.2 Electrochemical characterization of graphene modified carbon nanosheets

Encouraged by the excellent properties of our samples, we modified a glassy carbon electrode using GMCNs with different sheet thickness for analysing trace amounts of Pb(II) by SWASV in water. Fig. 3 shows the SWSVA response of different samples towards aqueous Pb(II) solutions with different concentrations,

Table 1 Structure parameters of the GMCN

Sample	S_{BET} [a] ($cm^2\ g^{-1}$)	S_{mic} [b] ($cm^2\ g^{-1}$)	V_{mic} [b] ($cm^3\ g^{-1}$)	V_{total} [c] ($cm^3\ g^{-1}$)	Sheet thickness (nm)
GMCN-1	431	304	0.14	0.54	10 ± 2
GMCN-2	520	410	0.19	0.41	20 ± 2
GMCN-3	576	491	0.23	0.33	34 ± 4
GMCN-4	621	503	0.33	0.37	72 ± 6

[a] S_{BET}: specific surface area calculated by the BET method. [b] S_{mic} and V_{mic}: micropore surface area and micropore volume calculated by the *t*-plot method. [c] V_{total}: total pore volume at $P/P_0 = 0.97$.

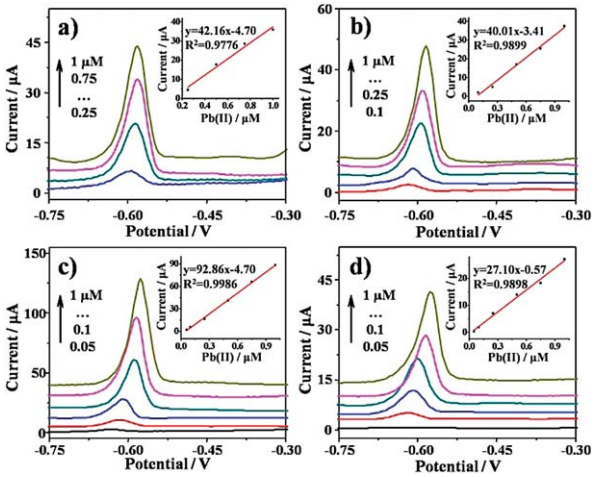

Fig. 3 SWASV response (background current was subtracted) of GMCN modified electrodes for analysis of Pb(II) over a concentration range of 0.05 to 1 μM. (a) GMCN-1, (b) GMCN-2, (c) GMCN-3, and (d) GMCN-4. Preconcentration time: 8 min; stripping solution: 0.01 M HAC and NaAC. SWASV conditions: frequency, 15 Hz, potential step, 4 mV and pulse amplitude, 25 mV. The insets are the calibration plots of the SWASV peak current *vs.* the concentration of Pb(II) ($R^2 > 0.9700$ for all).

and the corresponding calibration curves are derived accordingly. It can be seen that Pb(II) was detected at a potential of approximately −0.6 V with well-defined peaks, and the stripping peak current was proportional to the concentration of Pb(II) from 0.5 μM to 50 μM. The calibration curves of all the four GMCN modified electrodes exhibited a linear relationship ($R^2 > 0.9700$) between the peak current and the concentration of Pb(II) with a good regression coefficient.

It has been known that efficient preconcentration of Pb(II) on the chemically modified electrode is significant in stripping analysis. In other words, the excellent sensitivity and low limit of detection are strongly related to the adsorption capacity of the microporous carbon sheets. In this work, the sensing performance may be partly attributed to the high surface area of the samples, and the high surface area may provide more active sites for the capture of Pb(II). Besides the above reasons, the assembled hierarchical pore structure and exposed external surface area allow easy interaction with Pb(II) ions, leading to an enhanced adsorption rate.

3.3 Effect of electrical conductivity on sensitivity

Remarkably, the GMCN-modified electrodes showed an ultra-high sensitivity in the detection of Pb(II). It was found in Table 2 that, among the four samples, GMCN-4 with the thickest carbon sheets (72 ± 6 nm) delivered the lowest sensitivity of 27.10 μA μmol^{-1} towards Pb(II), whereas GMCN-1 with the thinnest sheets (10 ± 2 nm) showed a sensitivity up to 42.16 μA μmol^{-1}. GMCN-2 with the sheets of 20 ± 2 nm showed a moderate sensitivity of 40.01 μA μmol^{-1} which was very close to that of GMCN-1 but higher than that of GMCN-4. Interestingly, microporous carbon sheets, GMCN-3, having a moderate thickness gave the best sensitivity of 92.86 μA μmol^{-1}. This value was even higher than those of electrochemical sensors

Table 2 Electrochemical performance of the GMCN

Sample	Conductivity ($S\ cm^{-1}$)	LOD[a] (nM)	Sensitivity ($\mu A\ \mu M^{-1}$)	Sheet thickness (nm)
GMCN-1	19.8	50.20	42.16	10 ± 2
GMCN-2	9.1	15.31	40.01	20 ± 2
GMCN-3	1.2	1.12	92.86	34 ± 4
GMCN-4	0.8	0.65	27.10	72 ± 6
Porous Co_3O_4 (ref. 43)	—	18	71.57	—
P(DPA-*co*-2ABN)[44]	—	797	—	—
SnO_2/graphene[45]	—	0.1839	18.6	—

[a] LOD: the limit of detection.

based on the SnO_2/reduced graphene oxide nanocomposite[45] and γ-AlOOH (boehmite)@SiO_2/Fe_3O_4 porous magnetic microspheres.[11]

To further understand the mechanism that causes the different sensitivity of GMCNs, the effect of electrical conductivity on sensitivity was investigated by means of conductivity tests. As shown in Table 2, it was clear that all the samples exhibited relatively high electrical conductivity, and a significant increase in the electrical conductivity was obtained as the thickness of the carbon sheets decreased. It demonstrates that graphene sheets serve as conductive media in the hybrid carbon sheets, resulting in promotion of the electron transfer process at the modified electrode surface. Signal enhancement of a current may arise due to the good electrical conductivity of GMCNs. The sensitivity of all the samples increased in the order GMCN-4 < GMCN-2 < GMCN-1 < GMCN-3. The reason for the high sensitivity of GMCN-3 will be discussed as follows.

3.4 Effect of the surface area on LOD

In addition to the sensitivity, the limit of detection (LOD) is another important parameter that reflects the sensing performance towards Pb(II). With the method of 3σ, samples GMCN-1, GMCN-2 and GMCN-3 demonstrated a LOD of 50.20, 15.31, and 1.12 nM, respectively. In particular, it should be noted that the LOD of GMCN-4 was calculated to be 0.65 nM, which was significantly lower compared with that of GMCN-1 to GMCN-3, and the reported graphene-supported nanocomposites. The obtained LOD (0.13 ppb) was satisfactorily 2 orders of magnitude lower than the guideline value of 10 ppb in drinking water given by the World Health Organization. Therefore, the sensing performance of our GMCN is efficient for practical detection of Pb(II).

It should be pointed out that the decrease of LOD was consistent with the increase of carbon sheet thickness. The adsorption affinity to the target ions has been widely considered as one of the major factors controlling the LOD in detection of Pb(II). The results are probably due to that graphene sheets exhibit a relatively poor adsorption capacity towards Pb(II) but the microporous carbon supplies a large surface area and developed porosity. The large surface area and hierarchically interconnected pore system could provide a considerable number of adsorption sites, leading to the enhancement of adsorption capacity towards Pb(II). Especially in low concentration solutions, the thickest carbon sheets of GMCN-4 could accumulate a sufficient amount of Pb(II) on the electrode surface to produce a detectable signal owing to the high surface area. Therefore, Pb(II) can be detected efficiently on the GMCN-4 modified electrode with respect to the other electrodes. The results reveal that the LOD of sample GMCNs is directly proportional to the surface area. This indicates that the enlargement of the surface area is very favorable for lowering the LOD.

3.5 Comprehensive analysis

According to the abovementioned results, it seems that the two important performance parameters, namely the limit of detection and sensitivity, are strongly dependent on the specific surface area and electrical conductivity of the GMCN. However, neither the surface area nor the electrical conductivity alone could fully explain the electrochemical sensing performance of GMCNs. As a summary, we proposed the associations among the sensing performance parameters, electrical conductivity and the structure parameters. These are shown in Fig. 4.

As can be seen, GMCN-1 and GMCN-2 show moderate sensitivity and high LOD. Their low surface area may lead to a relatively poor adsorption affinity to Pb(II), that may partly lead to the high LOD. Another point that might be an important reason for the high LOD is the low signal-to-background ratio. Moreover, high electrical conductivity may amplify not only the analytical signals but also the background noise. In high concentration solutions, the value of background current is considered ignorable compared with the high signals. Nevertheless, the stripping peak current becomes weak (<1 μA) in the low concentration solution, resulting in the low signal-to-background ratio.[46,47] This

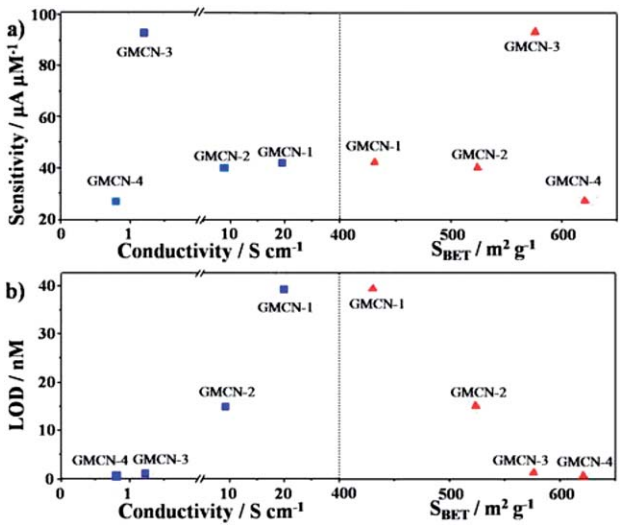

Fig. 4 (a) Blue squares indicate the relationship between the conductivity and sensitivity of GMCNs, and red triangles indicate the relationship between the surface area and sensitivity of GMCNs; (b) blue squares indicate the correlation between the conductivity and LOD of GMCNs, and red triangles indicate the correlation between the surface area and LOD of GMCNs.

may be the primary cause of the high LOD. Therefore, the relatively high values of background current show a serious interference for electrochemical detection of Pb(II), which limits the real application of the sensor.

GMCN-3 with a moderate electrical conductivity gives the best sensitivity towards Pb(II) with respect to the other three samples. This is probably due to the accessible high surface area that provides a considerable number of ion channels for electrochemical reactions and increases the adsorption affinity to Pb(II). On the other hand, the moderate electrical conductivity neither amplifies the background current to affect the LOD nor creates a barrier for electron transfer at the modified electrode surface. In contrast to other samples, GMCN-4 with a higher surface area delivers the poorest sensitivity and lowest LOD. The distinct performance of GMCN-4 further reveals that low electrical conductivity leads to a highly reduced background current, giving the lowest LOD, but decreases the stripping peak current. This is unfavorable for practical sensing.

On the basis of the above analyses, it can be found that the LOD lowered with an increase in surface area and a decrease in electrical conductivity. Meanwhile, GMCN-3 with a moderate electrical conductivity and relatively high surface area gave the best sensitivity. The results demonstrate that the combination of a suitable electrical conductivity and high surface area allows high adsorption capacity towards Pb(II), high signal-to-background ratio, favorable electron and ion channels for electrochemical reactions, thus significantly improving the electrochemical sensing performance in detection of Pb(II).

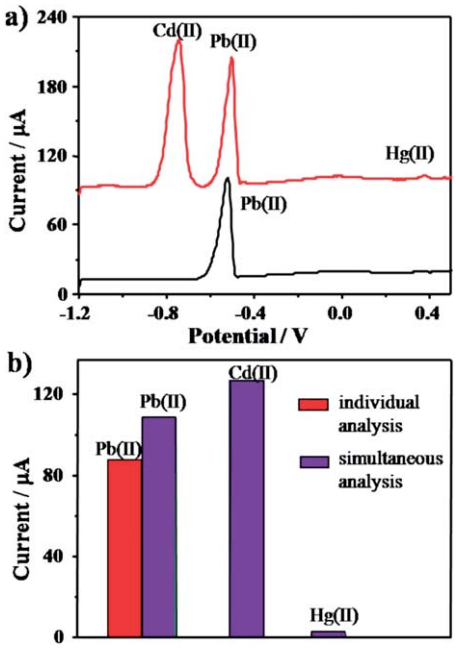

Fig. 5 (a) The red line indicates the SWASV response of the GMCN-3 modified electrode for the simultaneous analysis of Cd(II), Pb(II) and Hg(II). The black line indicates the SWASV response of the GMCN-3 modified electrode for the individual analysis of Pb(II); (b) differences in terms of SWASV response towards each metal ion when comparing individual with simultaneous analysis. The concentration for each metal ion is 1 μM.

3.6 Evaluation of mutual interferences

The SWASV response for the simultaneous analysis of Cd(II), Pb(II) and Hg(II) using the GMCN-3 modified electrode is displayed in Fig. 5a. GMCN-3 was applied to the determination of Pb(II) in the presence of Cd(II) and Hg(II). It shows individual peaks at approximately −0.8, −0.55, and 0.35 V for Cd(II), Pb(II) and Hg(II), respectively, in their coexistence. The separation between the stripping peak is large enough, and thus the selective detection for Pb(II) using the GMCN-3 modified electrode is feasible.

Significant differences were observed in Fig. 5b when comparing individual with simultaneous analysis. For simultaneous analysis, the stripping peak current (126.80 μA) of 1 μM Cd(II) was significantly higher than that of 1 μM Hg(II) (2.64 μA). Obviously, the stripping peak current (108.70 μA) of 1 μM Pb(II) in the presence of Cd(II) and Hg(II) is higher compared with individual analysis (87.63 μA). This result was likely due to the formation of the Pb film followed by the formation of Pb–Hg intermetallic compounds during the deposition step,[45] which gave the strong stripping signals toward ultratrace detection of Pb(II).

4 Conclusions

In the present study, a strategy based on the graphene modified carbon nanosheets has been developed for sensitive detection of trace amounts of Pb(II) in an aqueous solution. The experimental results suggest that the GMCN is a promising material which possesses the advantages of both porous carbon and graphene sheets to give rise to the accumulation of Pb(II) and electronic transport properties. By means of a wide tuning range of carbon layer thickness, the sensitivity of GMCN-3 towards Pb(II) is as high as 92.86 μA μmol^{-1}, which is higher than those of some sensors based on the SnO_2/reduced graphene oxide nanocomposite and γ-AlOOH (boehmite)@SiO_2/Fe_3O_4 porous magnetic microspheres, and the LOD can reach 1.12 nM, which is lower than the guideline value in drinking water given by the World Health Organization. The superior sensing performance can be attributed to the compromise of suitable electrical conductivity and high surface area. Finally, our study suggests that this concept on adsorption capacity, electrical conductivity and sensing behavior is very useful for the design of new sensing materials.

Acknowledgements

The financial support from the Special Program for Basic Research of the Ministry of Science and Technology (no. 2012CB626802) and National Science Fund for Distinguished Young Scholars (no. 21225312) is appreciated.

Notes and references

1 I. Turyan and D. Mandler, *Nature*, 1993, **362**, 703–704.
2 H. P. Wu, *Anal. Chem.*, 1996, **68**, 1639–1645.
3 Y. Kim, R. C. Johnson and J. T. Hupp, *Nano Lett.*, 2001, **1**, 165–167.

4 S. Barman and M. Sadhukhan, *J. Mater. Chem.*, 2012, **22**, 21832.
5 J. Gong, T. Zhou, D. Song, L. Zhang and X. Hu, *Anal. Chem.*, 2010, **82**, 567–573.
6 G. Martinez-Paredes, M. B. Gonzalez-Garcia and A. Costa-Garcia, *Electrochim. Acta*, 2009, **54**, 4801–4808.
7 R. Ojani, E. Ahmadi, J. B. Raoof and F. Mohamadnia, *J. Electroanal. Chem.*, 2009, **626**, 23–29.
8 M. Sadhukhan and S. Barman, *J. Mater. Chem. A*, 2013, **1**, 2752–2756.
9 M. Heitzmann, C. Bucher, J. C. Moutet, E. Pereira, B. L. Rivas, G. Royal and E. Saint-Aman, *Electrochim. Acta*, 2007, **52**, 3082–3087.
10 Y. X. Zhang, X. Y. Yu, Z. Jin, Y. Jia, J. H. Liu and X. J. Huang, *J. Mater. Chem.*, 2011, **21**, 16550–16557.
11 Y. Wei, R. Yang, Y. X. Zhang, L. Wang, J. H. Liu and X. J. Huang, *Chem. Commun.*, 2011, **47**, 11062–11064.
12 I. Willner, B. Willner and E. Katz, *Bioelectrochemistry*, 2007, **70**, 2–11.
13 P. Pandey, M. Datta and B. D. Malhotra, *Anal. Lett.*, 2008, **41**, 159–209.
14 F. Valentini and G. Palleschi, *Anal. Lett.*, 2008, **41**, 479–520.
15 L. S. Zhang, W. Li, Z. M. Cui and W. G. Song, *J. Phys. Chem. C*, 2009, **113**, 20594–20598.
16 A. Walcarius, *Trends Anal. Chem.*, 2012, **38**, 79–97.
17 Y. Zhang, J. Zhang, Y. Liu, H. Huang and Z. Kang, *Mater. Res. Bull.*, 2012, **47**, 1034–1039.
18 S. Su, W. Wu, J. Gao, J. Lu and C. Fan, *J. Mater. Chem.*, 2012, **22**, 18101–18110.
19 E. S. Forzani, X. Li, P. Zhang, N. Tao, R. Zhang, I. Amlani, R. Tsui and L. A. Nagahara, *Small*, 2006, **2**, 1283–1291.
20 C. E. Banks and R. G. Compton, *Anal. Sci.*, 2005, **21**, 1263–1268.
21 K. Wu, S. Hu, J. Fei and W. Bai, *Anal. Chim. Acta*, 2003, **489**, 215–221.
22 Y. Liu, Y. Li and X. P. Yan, *Adv. Funct. Mater.*, 2008, **18**, 1536–1543.
23 J. Wang, S. B. Hocevar and B. Ogorevc, *Electrochem. Commun.*, 2004, **6**, 176–179.
24 R. F. Service, *Science*, 2009, **324**, 875–877.
25 A. K. Geim and K. S. Novoselov, *Nat. Mater.*, 2007, **6**, 183–191.
26 S. Park and R. S. Ruoff, *Nat. Nanotechnol.*, 2009, **4**, 217–224.
27 M. D. Stoller, S. Park, Y. Zhu, J. An and R. S. Ruoff, *Nano Lett.*, 2008, **8**, 3498–3502.
28 M. Pumera, A. Ambrosi, A. Bonanni, E. L. K. Chng and H. L. Poh, *TrAC, Trends Anal. Chem.*, 2010, **29**, 954–965.
29 M. A. Worsley, P. J. Pauzauskie, T. Y. Olson, J. Biener, J. H. Satcher, Jr and T. F. Baumann, *J. Am. Chem. Soc.*, 2010, **132**, 14067–14069.
30 Z. S. Wu, Y. Sun, Y. Z. Tan, S. Yang, X. Feng and K. Müllen, *J. Am. Chem. Soc.*, 2012, **134**, 19532–19535.
31 X. Zhang, Z. Sui, B. Xu, S. Yue, Y. Luo, W. Zhan and B. Liu, *J. Mater. Chem.*, 2011, **21**, 6494–6497.
32 W. Zhang, J. Wei, H. Zhu, K. Zhang, F. Ma, Q. Mei, Z. Zhang and S. Wang, *J. Mater. Chem.*, 2012, **22**, 22631–22636.
33 B. Wang, B. Luo, M. Liang, A. Wang, J. Wang, Y. Fang, Y. Chang and L. Zhi, *Nanoscale*, 2011, **3**, 5059–5066.
34 Z. Q. Zhao, X. Chen, Q. Yang, J. H. Liu and X. J. Huang, *Electrochem. Commun.*, 2012, **23**, 21–24.
35 H. G. Sudibya, Q. He, H. Zhang and P. Chen, *ACS Nano*, 2011, **5**, 1990–1994.
36 Z. Q. Zhao, X. Chen, Q. Yang, J. H. Liu and X. J. Huang, *Chem. Commun.*, 2012, **48**, 2180–2182.
37 E. Auer, A. Freund, J. Pietsch and T. Tacke, *Appl. Catal., A*, 1998, **173**, 259–271.
38 J. Li, S. Guo, Y. Zhai and E. Wang, *Electrochem. Commun.*, 2009, **11**, 1085–1088.
39 C. Gao, X. Y. Yu, R. X. Xu, J. H. Liu and X. J. Huang, *ACS Appl. Mater. Interfaces*, 2012, **4**, 4672–4682.
40 G. P. Hao, A. H. Lu, W. Dong, Z. Y. Jin, X. Q. Zhang, J. T. Zhang and W. C. Li, *Adv. Energy Mater.*, DOI: 10.1002/aenm. 201300383.
41 M. Gao, C. K. N. Peh, W. L. Ong and G. W. Ho, *RSC Adv.*, 2013, **3**, 13169–13177.
42 H. Huang, P. Chen, X. Zhang, Y. Lu and W. Zhan, *Small*, 2013, **9**, 1397–1404.
43 Z. G. Liu, X. Chen, J. H. Liu and X. J. Huang, *Electrochem. Commun.*, 2013, **30**, 59–62.
44 M. F. Philipsa, A. I. Gopalanb and K. P. Lee, *J. Hazard. Mater.*, 2012, **237**, 46–54.
45 Y. Wei, C. Gao, F. L. Meng, H. H. Li, L. Wang, J. H. Liu and X. J. Huang, *J. Phys. Chem. C*, 2012, **116**, 1034–1041.
46 W. F. Sokol and D. H. Evans, *Anal. Chem.*, 1981, **53**, 578–580.
47 J. Xu, B. Jiang, J. Su, Y. Xiang, R. Yuan and Y. Chai, *Chem. Commun.*, 2012, **48**, 3309–3311.